SAND2019-5823C

Zirconium metal-organic framework functionalized plasmonic sensor

J. Briscoe[a,b*], L. Appelhans[a], S. Smith[a], K. Westlake[a], I. Brener[a,b], and J. Wright[a,b]
[a]Sandia National Laboratories, 1515 Eubank Blvd SE, Albuquerque, NM, USA 87123;
[b] Center for Integrated Technologies, 1101 Eubank Blvd SE, Albuquerque, NM, USA 87123

ABSTRACT

The modern world has expanded and evolved in many ways, however, exposure to chemicals has remained a constant threat to personal health. The development of a highly sensitive and selective sensor which can be multiplexed to provide rapid analysis capability in a cluttered sensing environment is desperately needed. We have investigated Zr-based metal-organic frameworks (MOFs) which demonstrate unique chemical properties in the presence of chemicals of interest. We present the development of an optimized plasmonic transducer coupled with a Zr-based MOF UiO-66 active layer. We will discuss the integration and characterization of the MOF/plasmonic sensor and summarize our results which show that, upon exposure to the COI, small changes in the optical characteristics of the MOF layer are effectively transduced by observing shifts in plasmonic resonance. The resulting sensor serves as an important first step towards the rapid detection, classification, and identification of chemical threats.

Keywords: surface plasmon polariton, metal-organic framework, optical sensor, chemical sensor
*jlbrisc@sandia.gov

1. INTRODUCTION

Traditional plasmonic based devices have been widely studied and have demonstrated success across multiple scientific disciplines. Sensing [1-7], biosensors [8-11], surface-enhanced Raman spectroscopy [12-14], cancer diagnosis [15], and enhanced photodetection [16, 17]. The unique ability to enhance light-matter interactions makes further study in plasmonics appealing.

Exposure to chemicals in everyday life is now more prevalent than ever [18]. Air and water pollution can be delivery mechanisms for toxins, carcinogens, and other chemicals of interest (COI). A compact, multiplexed, chemical sensor with high responsivity and selectivity is desperately needed. In this paper, we demonstrate the integration of Zr-based metal organic frameworks (MOFs) with a plasmonic transducer to demonstrate a nanoscale optical sensor that is highly sensitive to the presence of the COI. MOFs are porous coordination polymers where a central metal or metal-oxo cluster is coordinated by organic ligand forming a lattice and resulting in an ordered structure with nano- to micro-porosity, high surface area, and precise structural tunability. These properties make MOFs an ideal candidate for gaseous chemical sensing, however, transduction of a signal which probes changes in MOF films has been difficult. Plasmonic sensors have performed well in many sensing environments but have had limited success detecting gaseous chemical analytes at low levels [19-21]. This is due, in part, to the volume of molecules required to interact with the functionalized surface and produce a detectable shift in plasmonic resonance frequency. In this paper we demonstrate a qualitative demonstration of dimethyl methylphosphonate (DMMP) detection by a MOF functionalized plasmonic sensor.

2. METHODOLOGY

The field of biosensing has readily embraced plasmonic devices taking advantage of enhanced light-matter interactions to enhance refractive index sensitivity [1-7]. Traditionally a plasmonic surface is functionalized with a bio-transducer layer specifically designed to interact with a chosen analyte. A popular design used to measure changes in the bio-layer is to employ an artificially structured surface known as a nanohole array (NHA) as shown in Figure 1. The fabricated sensor is comprised of a pattern of 2D periodic nanoholes functionalized with a solvothermally deposited MOF layer. Incoming photons are converted to surface plasmon (SP) waves bound to the nanostructured surface. Excited SP waves experience radiative decay into a forward propagating wave resulting in enhanced optical transmission. This process of excitation-radiation can be spectrally monitored in the far-field as an extraordinary optical transmission (EOT) peak [22-26]. Surface

plasmons, excited at the metal-dielectric interface, are extremely sensitive to phase matching conditions. Changes in the refractive index of the dielectric layer result in shifts in plasmonic resonance which manifest as a change in the EOT peak.

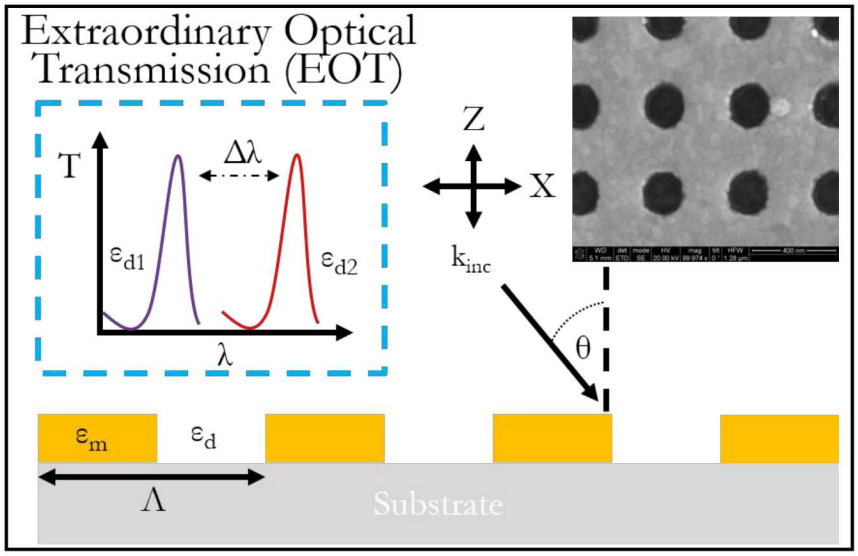

Figure 1. Schematic for EOT-based sensing. Incident photons are converted to SP waves at metal/dielectric interface. Changes in surface conditions can be monitored by observing the far-field EOT spectral response. Inset – SEM image of a fabricated NHA.

2.1 NHA design and fabrication

Due to the advances in lithographic techniques the spectral response of patterned nanostructures can be set through the application of known design parameters [24-26]. The expected position of an EOT peak can be determined by solving the excitation condition given by

$$\beta = k_{inc} \sin(\theta) \pm m \frac{2\pi}{\Lambda} \quad (1)$$

where β is the wave vector of the SP wave, k_{inc} is the wave vector of incident waves, θ is the angle of incidence, m is an integer, and Λ is the period of the nanostructure array.

Fabrication of the array was performed as follows. First a microscope slide was diced and cleaned under a high power O_2 plasma clean to remove any contaminants. A negative tone photoresist, ma-N 2403, was drop cast on the glass substrate and spun for 30 seconds at 5,000 RPM and then baked on a hot plate at 90 °C for 60 seconds. The resulting film thickness was approximately 150 nm thick. A JEOL electron beam lithography tool was used to define the patterned array under beam conditions of 100 kV acceleration voltage and 6 nA beam current with a base dose of 400 μC/cm^2. Post exposure, the sample was immersed for 60 seconds in MF-319 photodeveloper, rinsed in deionized (DI) water, and dried under an N_2 stream. Electron beam deposition was performed to deposit a layer of Ti/Au (5 nm/80 nm). The sample was then placed in a heated Remover PG bath (70 °C) for one hour to assist in metal lift-off. The final structure was a 1 mm x 1 mm NHA with hole size of 200 nm and periodicity of 400 nm.

2.2 Experimental setup

The experimental setup was designed to provide linear polarization control and a confocal imaging capability while exciting SP waves on the nanopatterned surface and collecting the spectral response of the EOT. The final design is shown

in Figure 2. The Excitation portion employed a quartz-tungsten halogen lamp (Thorlabs) which was focused, and end-fire coupled into a large core light pipe. This beam was then collimated, passed through a linear polarizer, and a 50:50 polka-dot beamsplitter. One section of the split beam was projected onto the focal plane of a CCD camera (Thorlabs) to provide front-side imaging and the other section was incident on the entrance aperture of an M Plan Apo NIR Mitutoyo 20x objective (NA 0.40). The objective focused the broadband light source onto the sample to a spot size of approximately 300 µm. The sample was mounted on a vertical X-Y stage which allowed fine control over excitation/collection locations on the fabricated NHA. A matching microscope objective was used to collect the transmitted spectrum and provide backside imaging of the sample. The Collection side of the setup is nearly identical to the Excitation side, terminating with the collection of the transmitted signal by a fiber-coupled Ocean Optics UV-VIS spectrometer.

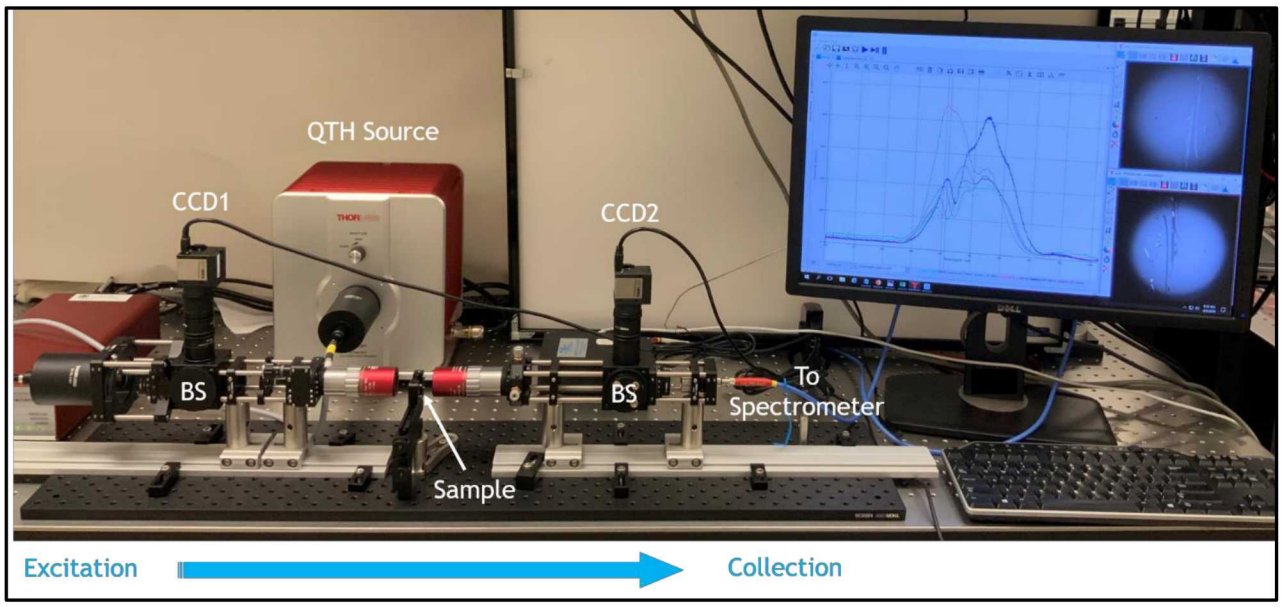

Figure 2. Schematic for Excitation/Collection experimental setup. This setup provided fine control over excitation and collection locations on the sensor and confocal imaging capability.

2.3 NHA device characterization

Characterization of the fabricated NHA was performed by introducing solutions of known refractive and plotting the resulting spectrum. Wavelength interrogation was chosen for these measurements. The chemicals used were DI water and the following laboratory grade chemicals: methanol, isopropanol, and ethylene glycol. The sample was rinsed thoroughly with DI water and dried under a compressed air stream after each introduction of analyte. A comparison of refractive index change to spectral shift provides an approximate measure of sensitivity of the fabricated sensor. The Zr-MOF UiO-66 was characterized with this method on a fabricated NHA sensor as well resulting in an estimated refractive of 1.437. However, further characterization of future MOF films on NHA samples are required to develop confidence in the estimated refractive index. Spectral results and a linear fit of the approximate sensitivity of the sensor are shown in Figure 3. Our sensitivity calculation is well within expected values found in literature [9, 19, 23].

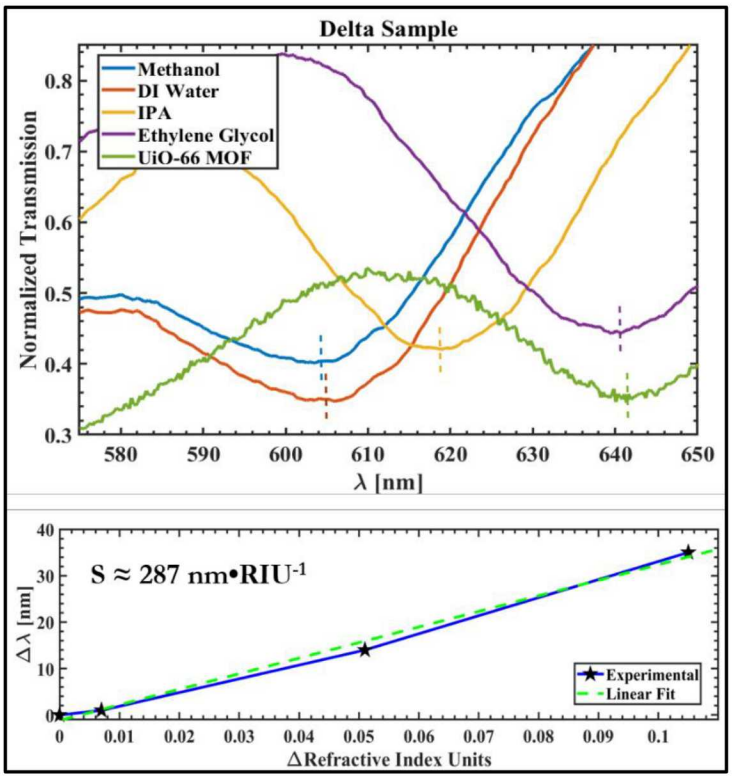

Figure 3. Top - Normalized transmitted intensity spectrum of the fabricated NHA after introduction of known analytes. The dotted lines indicate the curve minimum where the EOT peak was monitored. Bottom – Linear fit of experimental data.

2.4 Solvothermal growth of UiO-66

Many variations of the basic synthesis of UiO-66 exist in literature [27-30]. For this work we have explored four published synthetic methods. Each method varied important parameters such as: reagent concentration in solvent, use and stoichiometry of monoacid capping agents, water concentration, and heating methods. After many iterations our most successful process for solvothermal deposition of thin-film UiO-66 is based on that reported by Taddei et al. [27]. Representative films from our process are shown in Figure 4 along with a summary of the important parameters for deposition. Each UiO-66 film was grown on a glass or Si substrate covered in an 80-100 nm Au film. To our knowledge, this is the first demonstration of UiO-66 film growth on a Au surface. Typical film growths showed a strong interconnective behavior as film thicknesses reached 55-80 nm. X-ray diffraction (XRD) was performed to confirm the film was UiO-66 and is shown in Figure 4 as well.

The films showed varying levels of larger crystalline overgrowth, much of which could be removed by sonication, however, some large crystals remain, as can be seen in Figure 4. In a typical procedure zirconium (IV) chloride (290 mg, 1.24 mmol) was added gradually to 5 mL dimethylformamide (DMF) and sonicated to dissolve. Meanwhile 1,4-benzene dicarboxylic acid (230 mg, 1.27 mmol) was added to a separate 5 mL portion of DMF and stirred until dissolved. The two solutions were combined and acetic acid (2.1 mL) and water (135 µL) are added, in that order. The reaction mixture is stirred for 2-3 minutes and then placed into microwave vials with a Au/Si or Au/glass substrate, Au side up. The reaction is heated in the microwave reactor to 120 °C for 30 min. CAUTION: There is often pressure build-up during this reaction, use appropriately designed and rated equipment to accommodate greater-than-ambient pressures. After the reaction the substrate is removed from the reaction solution, rinsed thoroughly with DMF and placed in 2-3 mL fresh DMF overnight. The DMF is then exchanged for methanol (MeOH) and the substrate is further incubated overnight. Finally, the substrate is removed from MeOH, air dried, then placed in a vacuum oven at 90 °C overnight.

This process was repeated on fabricated NHA sensors as a transducer layer for functionalization to DMMP. Results of the functionalization process are shown in Figure 5. Although the interconnected conformal growth evident on planar Au films is not evident, close inspection of the NHA sensors shows obvious film growth and the presence of UiO-66 crystallite overgrowth within the nanoholes. Further investigation into the behavioral change of film growth on planar versus a periodic NHA surface is required.

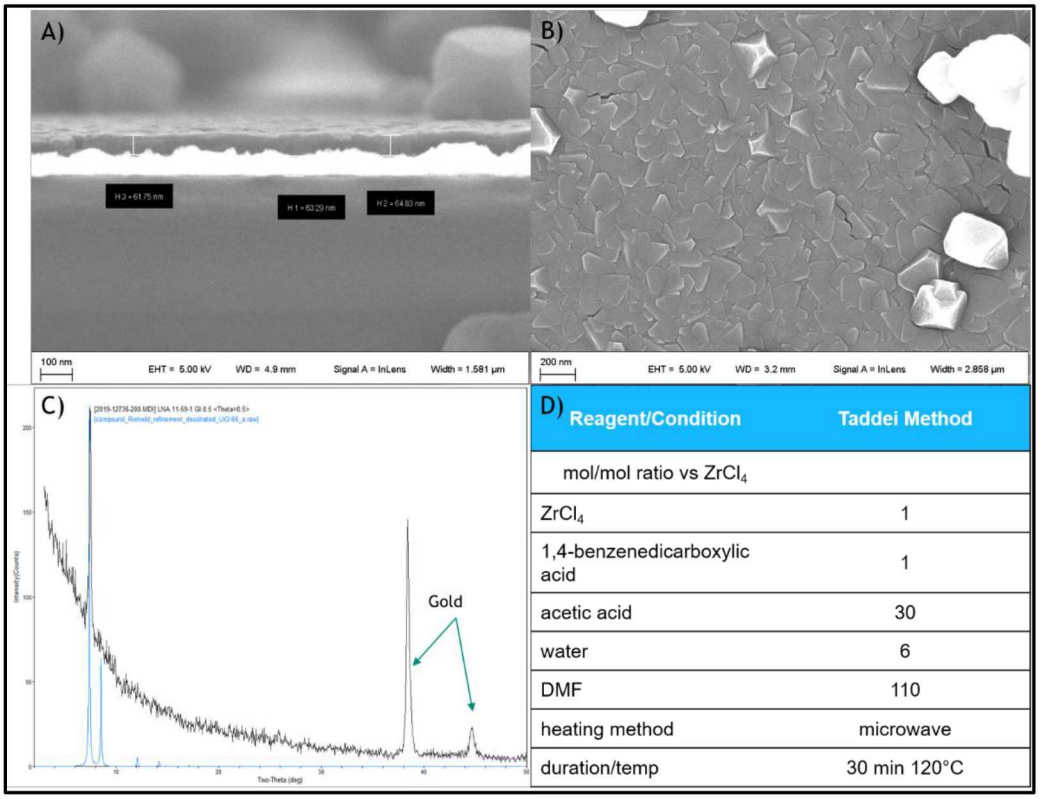

Reagent/Condition	Taddei Method
mol/mol ratio vs $ZrCl_4$	
$ZrCl_4$	1
1,4-benzenedicarboxylic acid	1
acetic acid	30
water	6
DMF	110
heating method	microwave
duration/temp	30 min 120°C

Figure 4. A) Cross-sectional view of the MOF film grown on a Si substrate covered in an 80 nm Au film. B) Top-down view of the film demonstrating interconnected crystal growth. C) XRD measurement confirming UiO-66 MOF film. D) Summary of important parameters/methods for MOF film solvothermal deposition.

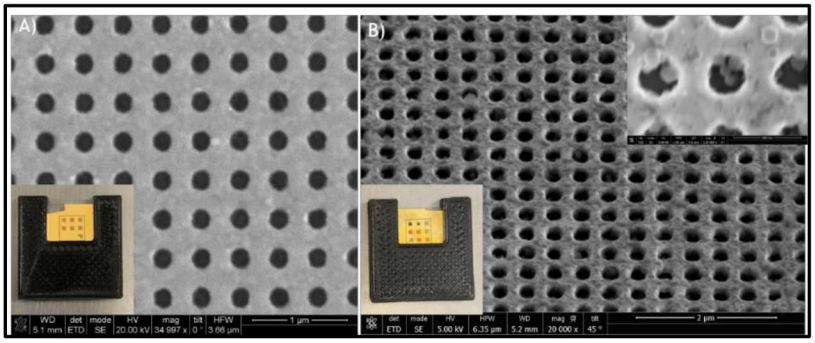

Figure 5. A) Fabricated NHA prior to MOF thin-film deposition. Inset – Far-field image of NHA sensor. B) NHA sensor post MOF processing. Left Inset – Far-field image of MOF functionalized NHA sensor. Right Inset – High magnification of NHA showing crystallite formation.

3. RESULTS

UiO-66 MOFs have been widely studied in literature and have demonstrated many interesting properties. At its base, a MOF is a crystalline coordination polymer with an extremely large surface area. With appropriate changes in chemistry the MOF can be synthesized to alter porosity from the nano- to micro-scale. UiO-66 has demonstrated sensitivity to DMMP and has been used as a sorber/concentrator [31, 32] and recently as a decomposition method for phosphonate simulants [34]. As noted earlier, a major shortfall of NHA sensors is their limited responsivity in a gas sensing environment. The integration of a MOF gas 'sponge' with a plasmonic refractive index sensing architecture should create a hybrid gas sensor with low-limit detection of DMMP. The following is a qualitative demonstration of this sensitivity and is an important first step towards demonstrating the MOF functionalized NHA sensor.

3.1 MOF sensing of DMMP

In traditional plasmonic sensing platforms small changes of refractive index within the sensing volume are transduced into a change in transmitted spectral response. Tracking this shift provides insight as to surface conditions of the plasmonic surface. For example, a NHA sensor functionalized with antibodies raised against specific antigens will detect antibody-antigen binding as an increase of refractive index as compared to a baseline. This methodology is also employed for MOF functionalized NHA sensors. For our use the baseline is the transmitted spectrum post MOF film deposition. A simplified schematic is shown in Figure 6. Here the area of the MOF within the plasmonic sensing volume is comprised of the framework and open space characterized as an 'air region'. Changes within the framework, either from a collapse or collection of DMMP molecules will result in alteration in the effective medium of these 'air regions'. Changes in effective medium are transduced by the NHA sensing platform.

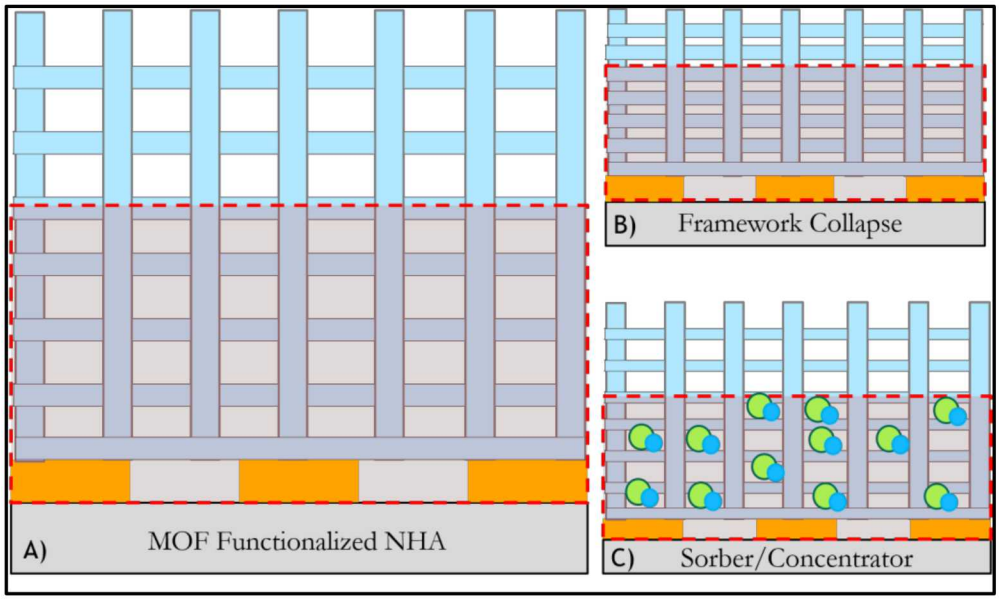

Figure 6. A) Simplified schematic representing the MOF functionalized NHA. The shaded red area represents the sensing volume of the sensor. B) Exposure to DMMP has been shown to collapse the linking framework of UiO-66 resulting in a refractive index increase within the sensing volume. C) UiO-66 has also demonstrated sorber/concentrator behavior in the presence of DMMP. This sensing method relies on trapping DMMP vapor molecules close to the sensing surface thereby changing the refractive index within the sensing volume.

3.2 Results of DMMP exposure

Two NHA sensors were functionalized with a UiO-66 MOF thin-film and characterized to determine baseline. A series of exposures was performed on the functionalized sensors and is summarized in Figure 7. The first sensor was exposed to liquid DMMP, the transmitted spectrum recorded, and then rinsed with DI water and dried under compressed air. We

observed a strong shift in the spectral response due to the change in refractive index caused by liquid DMMP in contact with the sensor interface. After the sensor was rinsed and dried a permanent red-shift in the spectral response remained. This cycle was performed three times, however, the spectrum never returned to baseline indicating a permanent change in the refractive index of the effective medium within the sensing volume. We believe this may be caused by some collapse of the UiO-66 framework [34]. The second sensor was exposed to DMMP vapor. As seen in Figure 7 we observe a small but noticeable shift in the transmitted spectrum. The exposure process was also performed three times to ensure a similar red-shift was observed. We believe this shift is due to absorption of DMMP vapor molecules by the UiO-66 film within the sensing volume.

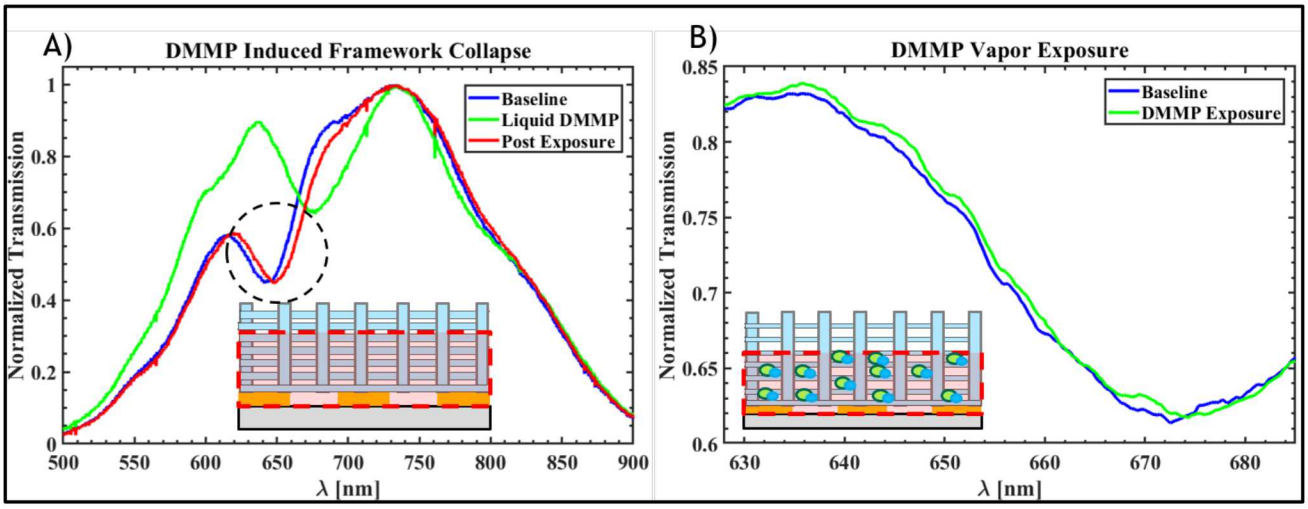

Figure 7. A) Normalized transmitted intensity of the functionalized NHA sensor after DMMP exposure. As indicated by the dotted circle, a permanent change in the spectral response has occurred. B) Spectral response of the sensor after DMMP vapor exposure. A small but noticeable shift in the transmitted spectrum confirming a qualitative demonstration of DMMP sensitivity.

4. CONCLUSION

We have presented a plasmonic sensor functionalized with a Zr-MOF (UiO-66). The NHA sensor was characterized and functionalized with a MOF transduction layer. To our knowledge this is the first successful hybridization of a plasmonic sensor with UiO-66 resulting in detection of both liquid and vapor DMMP. This is an important first step towards low-level detection of phosphonates in real-world scenarios.

5. ACKNOWLEDGEMENTS

This work was performed, in part, at the Center for Integrated Nanotechnologies, an Office of Science User Facility operated for the U.S. Department of Energy (DOE) Office of Science. Sandia National Laboratories is a multimission laboratory managed and operated by National Technology & Engineering Solutions of Sandia, LLC, a wholly owned subsidiary of Honeywell International, Inc., for the U.S. DOE's National Nuclear Security Administration under contract DE-NA-0003525. The views expressed in the article do not necessarily represent the views of the U.S. DOE or the United States Government.

This paper describes objective technical results and analysis. Any subjective views or opinions that might be expressed in the paper do not necessarily represent the views of the U.S. Department of Energy or the United States Government.

REFERENCES

[1] Stewart, M. E. et al., "Nanostructured plasmonic sensors," Chem. Rev., 108(2) 494–521(2008).

[2] Valsecchi, C. and Brolo, A. G., "Periodic metallic nanostructures as plasmonic chemical sensors," Langmuir 29(19), 5638–5649 (2013).

[3] Eftekhari, F. et al., "Nanoholes as nanochannels: Flow-through plasmonic sensing," Anal. Chem. 81(11), 4308–4311 (2009).

[4] Briscoe, J. L. and Cho, S.-Y., "A periodically coupled plasmon nanostructure for refractive index sensing," Opt. Exp. 19(9), 8815–8820 (2011).

[5] Briscoe, J. L. and Cho, S.-Y., "Hybrid plasmonic resonance for enhanced refractive index sensing," Electron. Lett. 47(23), 1294–1295 (2011).

[6] Briscoe, J. L., and Cho, S.-Y., and Brener, I., "Defect-assisted plasmonic crystal sensor," Opt. Lett. 38(14), 2569–2571 (2013).

[7] Homola J., Yee S. S., Gauglitz G., "Surface plasmon resonance sensors: Reviews," Sens. Actuators B Chem. 54, 3-15 (1999).

[8] Cho, S.-Y., Briscoe, J. L., Hansen, I. A., Smith, J. K., Chang, Y., and Brener, I., "Label-free plasmonic immunosensing for plasmodium in a whole blood lysate," IEEE Sensors J.,14 (5), 1399–1404 (2014).

[9] Hoa X.D., Kirk A.G., and Tabrizian M., "Towards integrated and sensitive surface plasmon resonance biosensors: A review of recent progress," Biosens. Bioelectron 23, 151–160 (2007).

[10] Liedberg, B., Claes, N., and Lundstrom, I. "Biosensing with surface plasmon resonance-how it all started." Biosens. Bioelectron. 10(8), 1-10 (1995).

[11] Yanik, A. A. et al., "An optofluidic nanoplasmonic biosensor for direct detection of live viruses from biological media," *Nano Lett.* 10(12), 4962–4969 (2010).

[12] Cui L., Wang P., Fang Y., Li Y., Sun M., "A plasmon-driven selective surface catalytic reaction revealed by surface-enhanced Raman scattering in an electrochemical environment," Sci. Rep. 5(11920), (2015).

[13] Wang D., Zhu W., Best M.D., Camden J.P., Crozier K.B., "Directional Raman scattering from single molecules in the feed gaps of optical antennas," Nano Lett. 13, 2194-2198 (2013).

[14] Lim D.K., Jeon K.S., Kim H.M., Nam J.M., Suh Y.D., "Nanogap-engineerable Raman-active nanodumbbells for single-molecule detection," Nat. Mater. 9, 60-67 (2010).

[15] Gao, D., Chen, W., Mulchandani, A., and Schultz, J. S. "Detection of tumor markers based on extinction spectra of visible light passing through gold nanoholes," Appl. Phys. Lett., 90(7), 073901-1–073901-3 (2007).

[16] Li, W., and Valentine, J., "Harvesting the loss: surface plasmon-based hot electron photodetection," Nanophotonics 6, 177-191 (2017).

[17] Li, W., and Valentine, J., "Metamaterial Perfect Absorber Based Hot Electron Photodetection," Nano Letters 14, 3510-3514 (2014).

[18] Institute of Medicine, "Identifying and Reducing Environmental Health Risks of Chemicals in Our Society: Workshop Summary," The National Academies Press, Washington, DC, (2014).

[19] Nylander C., Liedberg B., Lind T., "Gas detection by means of surface plasmon resonance," Sens. Actuators. 3, 79–88 (1982).

[20] Liedberg, B., Nylander, C., and Lunström, I., "Surface-plasmon resonance for gas-detection and biosensing," Sens. Actuators 4, 299–304 (1983).

[21] Wright, J., Cicotte, K.N., Subramania, G., Dirk, S., and Brener, I., "Chemoselective gas sensor based on plasmonic nanohole arrays," Optical Mat. Exp. 2(11), 1655-1662 (2012).

[22] De Leebeeck, A., Kumar, L. K. S., de Lange, V., Sinton, D., Gordon, R., and Brolo, A. G., "On-chip surface-based detection with nanohole arrays," Anal. Chem. 79(11), 4094–4100 (2007).

[23] Gordon, R., Sinton, D., Kavanagh, K. L., and Brolo, A. G., "A new generation of sensors based on extraordinary optical transmission," Acc. Chem. Res. 41(8), 1049–1057 (2008).

[24] Ebbesen, T. W., Lezec, H. J., Ghaemi, H. F., Thio, T., and Wolff, P. A., "Extraordinary optical transmission through sub-wavelength hole arrays," Nature 391(6668), 667–669 (1998).

[25] Genet, C. and Ebbesen, T. W., "Light in tiny holes," Nature 445(7123), 39–46 (2007).

[26] Martín-Moreno, L., García-Vidal, F. J., Lezec, H. J., Pellerin, K. M., Thio, T., Pendry, J. B., and Ebbesen, T. W. "Theory of extraordinary optical transmission through subwavelength hole arrays," Phys. Rev. Lett. 86(6), 1114–1117 (2001).

[27] Taddei, M., Dau, P.V., Cohen, S.M., Ranocchiari, M., van Bokhoven, J.A., Constantino, F., Sabatini, S., and Vivani, R., "Efficient microwave assisted synthesis of metal-organic framework UiO-66: optimization and scale up," Dalton Trans. 44(31), 14019-14026 (2015).
[28] Miyamoto, M., Kohmura, S., Iwatsuka, H., Oumi, Y., and Uemiya, S., "*In situ* solvothermal growth of highly oriented Zr-based metal organic framework UiO-66 film with monocrystalline layer," CrystEngComm 17, 3422-3425 (2015)
[29] Fei, H., Pullen, S., Wagner, A., Ott, S., and Cohen, S.M., "Functionalization of robust Zr(IV)-based metal-organic framework films *via* a postsynthetic ligand exchange," Chem. Commun. 51, 66-69 (2015).
[30] Katz, M.J., Brown, Z.J., Colon, Y.J., Hupp, J.T., and Farha, O., "A facile synthesis of UiO-66, UiO-67, and their derivatives," Chem. Commun. 49, 9449-9451 (2013).
[31] Ni Z., Jerrell, J.P., Cadwallader, K.R., and Masel, R.I., "Metal−Organic Frameworks as Adsorbents for Trapping and Preconcentration of Organic Phosphonates," Anal. Chem. 79(4), 1290-1293 (2007).
[32] Barea, E., and Navarro, J.A.R., "Capture of Nerve Agents and Mustard Gas Analogues by Hydrophobic Robust MOF-5 Type Metal–Organic Frameworks," J. Am. Chem. Soc. 133(31), 11888-11891 (2011).
[33] Stassen, I. et al., "Towards metal-organic framework based field effect chemical sensors: UiO-66-NH_2 for nerve agent detection," Chem. Sci 7(9), 5827-5832 (2016).
[34] Plonka, A.M., Wang, Q., Gordon, W.O., Balboa, A., Troya, D., Guo, W., Sharp, W., Morris, J.R., Hill, C.L., and Frenkel, A., "In Situ Probes of Capture and Decomposition of Chemical Warfare Agent Simulants by Zr-based Metal Organic Frameworks," J. Am. Chem. Soc. 139(2), 599-602 (2017).